Atmospheric Environment 96 (2014) 370–379

Contents lists available at ScienceDirect

Atmospheric Environment

journal homepage: www.elsevier.com/locate/atmosenv

Observations of new particle formation at two distinct Indian subcontinental urban locations

V.P. Kanawade [a, *], Sachchida N. Tripathi [a, *], Devendraa Siingh [b], Alok S. Gautam [b], Atul K. Srivastava [c], Adarsh K. Kamra [b], Vijay K. Soni [d], Virendra Sethi [e]

[a] Department of Civil Engineering, Indian Institute of Technology, Kanpur, India
[b] Indian Institute of Tropical Meteorology, Pune, India
[c] Indian Institute of Tropical Meteorology (Branch), Prof Ramnath Vij Marg, New Delhi, India
[d] India Meteorological Department, Lodhi Road, New Delhi, India
[e] Center for Environmental Science and Engineering, Indian Institute of Technology Bombay, Mumbai, India

HIGHLIGHTS

- New particle formation was observed at both urban locations in India.
- The properties of ultrafine particles during new particle formation were studied.
- Particle formation and growth rates showed different patterns at these urban sites.
- The particle mode diameter at Kanpur was larger than at Pune.

ARTICLE INFO

Article history:
Received 24 March 2014
Received in revised form
30 July 2014
Accepted 1 August 2014
Available online 1 August 2014

Keywords:
Particle size distribution
Ultrafine particles
Formation rate
Growth
Urban

ABSTRACT

While the formation of new atmospheric aerosol particles and their subsequent growth have been observed under diverse environmental conditions globally, such observations are very scarce over Indian subcontinent. Here, we present the systematic analysis for new particle formation (NPF) from two distinct urban locations in India during April–May of two consecutive years. Particle size distributions were measured at Pune (18.53°N, 73.85°E) during 16 April–23 May, 2012 and at Kanpur (26.46°N, 80.32°E) during 16 April–23 May, 2013. The campaign mean total particle number concentration in the similar size range of 4–135 nm at Pune (12.2×10^3 cm^{-3}) was higher than at Kanpur (7.9×10^3 cm^{-3}), whereas the estimated total condensation sink (CS_{4-750}) at Pune (16.2×10^{-3} s^{-1}) was lower than at Kanpur (33.3×10^{-3} s^{-1}). Despite lower particle number concentrations at Kanpur, larger particle sizes resulted in higher condensation sink than at Pune. The mean particle mode diameter at Kanpur was found larger by a factor of ~1.8 than at Pune. NPF events were observed commonly at both sites, with lower frequency at Kanpur (14%) than that at Pune (26%). The derived particle growth rates, *GR*, and the formation rates of 5 nm particles, J_5, ranged from 3.4 to 13.3 nm h^{-1} and 0.4 to 13.9 cm^{-3} s^{-1}, respectively, which are generally comparable to typical values reported in previous studies. Generally, the particle growth rates were found higher at Kanpur, whereas the formation rates were higher at Pune. It appears that the presence of pre-existing large particles at Kanpur than at Pune suppressed formation rates and favored particle growth. Overall, NPF occurred at lower condensation sink, lower RH, higher solar radiation, and higher temperature.

1. Introduction

Atmospheric aerosols influence the climate directly by scattering and absorbing incoming solar radiation (Schwartz, 1996), and indirectly by modifying cloud microphysical properties and lifetime via cloud condensation nuclei (CCN) activation (Twomey, 1991), thus affecting the Earth's radiation budget. One of the

* Corresponding authors.
E-mail addresses: vijaykanawade03@yahoo.co.in, vijaypk@iitk.ac.in (V.P. Kanawade), snt@iitk.ac.in (S.N. Tripathi).

http://dx.doi.org/10.1016/j.atmosenv.2014.08.001
1352-2310/

leading reasons for uncertainty in the aerosol indirect effect is ambiguity in the CCN budget (Pierce and Adams, 2009). The formation of aerosol particles (via gas-to-particle conversion) is one of the predominant sources for new particles in the atmosphere and thus is an important process that controls total aerosol number concentration and cloud abundance. New particle formation (NPF) is a global phenomenon, with newly formed particles accounting in the range of about 3–70% of CCN production in the troposphere (Merikanto et al., 2009; Pierce and Adams, 2009; Spracklen et al., 2008). Regional NPF events take place frequently in the continental boundary layer, wherein NPF occurs over a large spatial scale (Kulmala et al., 2012). Such events have been reported in numerous studies at diverse locations, including several urban locations (McMurry et al., 2005; Stanier et al., 2004; Yue et al., 2009). Despite these extensive studies, the processes involved in NPF are still not well understood.

The first direct observation of atmospheric nanoparticles and clusters down to 1 nm diameter only recently revealed that NPF occurs by forming stable critical cluster (diameter of 1.5 ± 0.3 nm), followed by subsequent growth of clusters to 2 and 3 nm (Kulmala et al., 2013). Sulfuric acid (H_2SO_4) is thought to be the primary vapor responsible for NPF because of its low vapor pressure (Sipilä et al., 2010). However, H_2SO_4 alone does not form stable clusters to initiate nucleation and other additional base compounds are necessary to stabilize these H_2SO_4 clusters, such as organic molecules (Schobesberger et al., 2013), ammonia (NH_3) (Kirkby et al., 2011) and amines (Paasonen et al., 2012), and facilitate them to grow into particles. Previous laboratory experiments have also revealed that NH_3 (Ball et al., 1999) and amines (Almeida et al., 2013; Dawson et al., 2012; Yu et al., 2011) play a crucial role in NPF and growth processes at atmospheric conditions. Further, organic acids and their low-volatility oxidation products (Metzger et al., 2010; O'Dowd et al., 2002; Zhang et al., 2004) and charged ion clusters (Kanawade and Tripathi, 2006; Lee et al., 2003; Yu and Turco, 2008) have also been suggested to initiate particle formation, though the latter component has a minor role in the boundary layer (Kirkby et al., 2011).

Most of the studies reported to date were conducted in the temperate regions where distinct and definitive seasonal variations in climatic conditions can be observed (Cheung et al., 2011; Kulmala et al., 2004; Mejía and Morawska, 2009; Vakkari et al., 2011). However, studies in tropical regions are still very limited (Betha et al., 2013; Iida et al., 2008; Kanawade et al., 2014; Siingh et al., 2013), where the climatic conditions are much different. In particular, over the Indian subcontinent, the systematic analysis for NPF are limited to only a few locations; New Delhi (Mönkkönen et al., 2005), Pune (Siingh et al., 2013), Gual Pahari (Hyvärinen et al., 2010), Gadanki (Kanawade et al., 2014), Kullu-Manali in the Western Himalaya (Sharma et al., 2011), Mukteshwar (Komppula et al., 2009; Neitola et al., 2011), and Hanle in the Trans-Himalayas (Moorthy et al., 2011). Therefore, we measured particle size distributions in the diameter range of 4–135 nm at Pune during April–May 2012. We have also conducted analogous measurements, for the first time, at Kanpur that show strong seasonality in climatic conditions, but in the size range of 4–750 nm and during April–May 2013. The objective of this study is to examine NPF characteristics at two distinct urban locations that have different climatic conditions and emission sources.

2. Experimental setup and methods

2.1. Measurement sites

Measurements were made at two distinct urban locations (Pune and Kanpur) in India (Fig. 1). While observations of NPF have only recently been reported from Pune (Siingh et al., 2013), there are currently no published reports from Kanpur. In Pune, the measurements were carried out from the second floor of the Indian Institute of Tropical Meteorology building (IITM, 18.53°N, 73.85°E, 573 m amsl). In Kanpur, these were carried out from the second floor of the Center for Environmental Science and Engineering building in Indian Institute of Technology campus (IIT, 26.46°N, 80.32°E, 125 m amsl).

The Pune site is located on the outskirts of Pune city (~5 km away from the city center to the northwest) with a population of ~9 million as per 2011 census report. This site is surrounded by hillocks about 500–800 m high amsl on three sides, forming a valley-type configuration. A road with moderate traffic is located about 100 m to the North of the site. This site has no major industrial

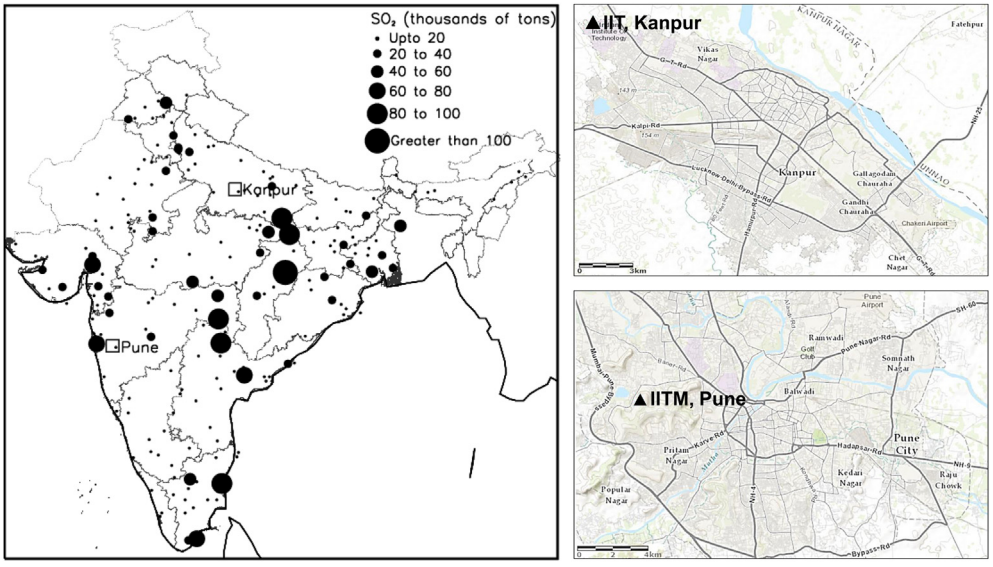

Fig. 1. Regional map showing location of the measurement sites, Pune and Kanpur (left panel). The industrial facilities SO_2 emissions for the year 2002 (dots) (Garg et al., 2002) are also indicated. The size of a dot corresponds to the emissions of the facility (in thousands of tons). The right panels show major road map in the immediate vicinity of each site (courtesy: www.arcgis.com).

activities within ~5 km radius but several large industrial facilities are located to the west and north within a radius of 500 km.

The Kanpur site is located on the outskirts of Kanpur city (~12 km away from the city center to the northwest) with a population of ~4.5 million as per 2011 census report. A road with a moderately heavy traffic is located about 600 m to the East of the site. This site is located in one of the biggest industrial hubs in the Indo-Gangetic plains (IGP) in Northern India, and a large number of coal-burning power plants are clustered along this area. This region continuously produces anthropogenic pollution from urban, industrial, and rural combustion sources, causing large primary aerosol loading throughout the year, with an increasing trend in aerosol optical depth (AOD) of 7.69% yr^{-1} over Kanpur for 2001–2010 (Kaskaoutis et al., 2012). This site is also heavily polluted compared to that of Pune (Table S1). Besides, Kanpur site is also affected by desert and alluvial dust particles during April–June months (Srivastava et al., 2012).

2.2. Sampling and instrumentation

Aerosol and gas instruments, sampling procedures, and data reduction methodologies were identical for both sites with a few exceptions noted below. At Pune, particle size distributions were measured with the scanning mobility particle sizer (SMPS) using a long-differential mobility analyzer (LDMA, TSI 3080) in combination with a butanol condensation particle counter (CPC, TSI 3776) during 20 March–15 April, 2012 and using a nano-DMA (NDMA, TSI, 3085) in combination with a butanol CPC (TSI 3775) during 16 April–23 May, 2012. The detectable aerosol mobility diameter ranged from 14 to 750 nm (112 size bins) and 4 to 135 nm (101 size bins) for LDMA and NDMA, respectively. At Kanpur, NDMA and LDMA were operated simultaneously to measure particle size distributions in a wide size range of 4–750 nm during 16 April–23 May, 2013. At both sites, the SMPS was set to down-scan 4 min and 45 s plus a wait-time of 15 s, thus producing one average particle size distribution every 5 min. The ambient air passed through a black conductive tube of 100 cm length and 0.54 cm inner diameter at a sample flow rate of 3.0 lpm (sheath flow rate of 0.3 lpm), and then passed through a 0.071 cm orifice impactor (cut-off diameter of 887 nm) to remove large particles entering into the SMPS and to minimize the particle losses. Weekly cleaning and greasing the impactor have also been conducted to avoid plausible clogging. While the hygroscopic growth effect may be significant for measurements at higher ambient relative humidity (Hamed et al., 2011), it was not controlled in our measurements for the reason that it is generally found to be relatively lower during pre-monsoon season (April–May) at both sites (e.g. <40%, Fig. S1b). Further, the size-dependent diffusional losses for the sampling line were also corrected using empirical function given by Baron and Willeke (2001). For our settings, the diffusion correction factor was about 55% and 10% for 5 nm and 20 nm size particles, respectively. Note that the counting efficiency of aerosol particles (e.g. Sucrose) for CPC (TSI 3775) drops down to 50% at the minimum detectable particle cut-off size (D_{50} = 4 nm). Further, the possibility of formation of liquid water in the sampling tube was minimized by using a short tube length, disconnecting it from the ambient air during rain and blowing it with clean air before use and also at regular time intervals.

Particle size distribution measurements are usually carried out using a combination of two or more SMPS systems to provide a wide particle size range of 3–1000 nm. Indeed, SMPS measurements at Kanpur provided particle size distributions in the size range of 4–750 nm. However, we did not have a LDMA operating simultaneously at Pune. The size-segregated particle concentrations were derived by integrating the number concentration of particles in the range of 5–25 nm (46 size bins), 25–100 nm (38 size bins), 100–750 nm (55 size bins), and 4–135 nm (101 size bins). These concentrations hereafter are denoted as N_{5-25}, N_{25-100}, $N_{100-750}$, and N_{4-135}, respectively. To ensure appropriate comparison between our sites, we report total particle number concentration in the similar diameter range of 4–135 nm whereas the condensation sink was estimated and calculated in the size range of 4–750 nm at Pune and Kanpur, respectively, hereafter denoted as CS_{4-750}. In order to estimate CS_{4-750} at Pune, in the absence of concurrent LDMA measurements, we have calculated merged particle size distribution in the size range of 4–750 nm from LDMA (before 16 April) and NDMA (after 16 April) measurements. The mean and standard deviation of CS_{4-750} derived from the merged particle size distribution is $(16.2 \pm 7.1) \times 10^{-3}$ s^{-1}, higher by a factor of 2.4 than that of NDMA measurements alone. We used this constant factor to estimate CS_{4-750} for NDMA measurements after 16 April 2012 at the Pune site. Sulfur dioxide (SO_2) was measured using a Thermo Environmental 43*i*-pulsed UV-fluorescence analyzer, with a detection limit of ~0.05 ppbv and an uncertainty of ±10%. The zero settings and span checks have been conducted at regular intervals for the best performance of SO_2 analyzer. Meteorological parameters such as air temperature, relative humidity (RH), wind speed, wind direction, and solar radiation were also measured simultaneously (Table S2). In order to investigate the transport directions against primary aerosol sources in the regional vicinity of the sampling sites, the Hybrid Single-Particle Lagrangian Integrated Trajectory (HYSPLIT) model calculated air mass backward trajectories, the Regional Emission inventory in Asia (REAS) estimated anthropogenic black carbon (BC) emissions and Moderate Resolution Imaging Spectrometer (MODIS) fire counts were also studied (Fig. S2).

Since the measurements were carried out during April–May of 2012 and 2013, we examined the variability in atmospheric conditions during these consecutive years at both sites. The origin and meteorological condition of air masses being an important factor in NPF (Kanawade et al., 2012; Sogacheva et al., 2007), we have calculated 3-day air mass backward trajectories arriving at 12:00 local time (LT) at 100 m above the surface at both sites. Fig. S1 shows the averaged diurnal variation of temperature, RH and solar radiation, and air mass history for each site and year. The observed mean minimum and maximum temperatures were also comparable to the climatological mean values at both the sites (Fig. S1a, e). Thus, it appears to us that the atmospheric conditions were comparable during these consecutive years at both sites.

2.3. NPF event classification

A comprehensive review of the current methods used to measure the particle size distribution and ultrafine particles, procedures, and ancillary tools for studying regional NPF events has recently been published by Kulmala et al. (2012). Briefly, NPF occurs in two distinct stages; formation of a critical cluster and subsequent growth of freshly nucleated particles to larger sizes (Kulmala et al., 2013; Zhang, 2010). Here, the NPF event was identified as an event when there was a significant increase in number concentrations of ultrafine particles in the size range of 5–25 nm (N_{5-25}) and these ultrafine particles grew larger in size for at least 3 h continuously, which is consistent with the NPF terminology used in the current literature. As a result, consecutive particle size distributions displayed a “banana” shaped growth, in a similar manner to Dal Maso et al. (2005) and Stanier et al. (2004). We also observed clean days with no evidence for increase in N_{5-25}, those were identified as nonNPF (i.e. no nucleation) events. The days with unexplained (or mixed) features were identified as unidentified NPF events.

2.4. Determination of particle growth rate, formation rate, and condensation sink

The condensational growth consumes a part of the condensable vapors from the atmosphere, and can be a controlling process, preventing further particle formation. A number of methods have been developed to estimate particle growth rates (e.g. Dal Maso et al., 2005; Kulmala et al., 2001). In this study, we used a straightforward approach given by Dal Maso et al. (2005). The average growth rate (GR) over a NPF event time duration was estimated by fitting a first-order polynomial line through the temporal variation of the particle mode diameter ($D_{p,\ mode}$) of the measured particle size distributions and calculating its slope.

The particle formation rate (J) is defined as the flux of the nucleated particles into the measured nucleation mode size range (i.e. 5–25 nm, in this study) (Kulmala et al., 2004). The empirical particle formation rate was determined by simplified approximation of the general dynamic equation (GDE), describing the evolution of particle size distribution (Seinfeld and Pandis, 2006). According to Dal Maso et al. (2005), the particle formation rate of 5 nm particles (J_5) can be estimated as follows:

$$J_5 = \frac{dN_{5-25}}{dt} + F_{coag} + F_{growth} \quad (1)$$

where F_{coag} is the flux due to coagulation losses, and F_{growth} is the flux of particles growing out of the nucleation mode size range. dN_{5-25}/dt is the rate of change of nucleation mode particles with time, t. It has to be noted that particles grew out of the freshly nucleated size range of 5–25 nm, as a result F_{growth} term in Eq. (1) can not be neglected and was calculated by Dal Maso et al. (2005) method as,

$$F_{growth} = \frac{1}{\Delta D_p} \cdot GR_{5-25} \cdot N_{5-25} \quad (2)$$

where, $\Delta D_p = (D_{p,\ 2} - D_{p,\ 1}) = (25 - 5) = 20$ nm

$$F_{growth} = \frac{1}{20\ nm} \cdot GR_{5-25} \cdot N_{5-25} \quad (3)$$

Here, GR_{5-25} was obtained from the SMPS data in the size range 5–25 nm, and N_{5-25} is the number concentration of nucleation mode particles. The coagulation loss for the size range 5–25, F_{coag}, was estimated as:

$$F_{coag} = N_{5-25} \cdot \sum_j K_{ij} \cdot N_j \quad (4)$$

where $\sum K_{ij} \cdot N_j$ is the coagulation sink. N_j is the particle number concentration of size bin j. K_{ij} is the coagulation coefficient between size bin i (i.e. the reference) and j, and is given as (Seinfeld and Pandis, 2006):

$$K_{ij} = 2\pi \cdot (d_i + d_j) \cdot (D_i + D_j) \cdot \beta_{F_{i,j}} \quad (5)$$

where d is the diameter of a size bin, D and β_F are the size dependent diffusion coefficient and Fuchs correction factor of particles, respectively.

The condensation sink (CS) determines how rapidly vapor molecules will condense onto existing particles and depends strongly on the shape of the particle size distribution. Here, CS was calculated as follows (Kulmala et al., 2001):

$$CS = 2\pi \cdot D_j \cdot \sum_j \beta_{m,j} \cdot d_j \cdot N_j \quad (6)$$

$$\beta_{m,j} = \frac{1 + Kn_j}{1 + 0.337Kn_j + \frac{4Kn_j}{3\alpha} + \frac{4Kn_j^2}{3\alpha}} \text{ and } Kn_j = \frac{2\lambda_v}{d_j}$$

where β_m is the size-dependent transition correction factor, Kn is the Knudsen number, D is the diffusion coefficient for H_2SO_4 (0.104 $cm^2\ s^{-1}$), α is mass accommodation coefficient (taken as unity), λ_v is the mean free path of H_2SO_4 molecule (6.7×10^{-6} cm).

3. Results and discussions

3.1. Observations of particle size distributions

Fig. 2 shows the hourly time variation of the measured particle size distributions, N_{4-135}, CS_{4-750}, and SO_2 at Pune and Kanpur. Note that there are no SO_2 and concurrent LDMA data available at the Pune site. The days with ultrafine particle bursts in the size range of 5–25 nm were observed at both sites. One typical NPF event day, which is marked by an open rectangle in Fig. 2, at each site is discussed in the following section. Table 1 gives the campaign mean, standard deviation, median, minimum and maximum of size-segregated particle number concentrations, CS_{4-750}, $D_{p,\ mode}$, and SO_2. N_{4-135} at Pune was $(12.2 \pm 6.2) \times 10^3$ cm^{-3}, higher than that at Kanpur, $(7.9 \pm 3.4) \times 10^3$ cm^{-3}. However, CS_{4-750} was higher at Kanpur $(33.3 \pm 8.7) \times 10^{-3}$ s^{-1}, to that at Pune, $(16.2 \pm 7.1) \times 10^{-3}$ s^{-1}, perhaps due to elevated anthropogenic sources in the IGP region (e.g. biomass/biofuel burning and cooking aside from traffic emissions), as indicated by strong emissions of black carbon (BC) and large number of fire hotspots over this region (Fig. S2). A previous study at Gual Pahari (New Delhi) in the IGP region also indicated that a high percentage of aerosol mass primarily consisted of BC (Hyvärinen et al., 2010). The mean and standard deviation of particle mode diameter at Kanpur was 86.2 ± 39.1 nm, which is about two-fold higher than that at Pune, 47.8 ± 22.1 nm.

3.2. New particle formation events and their characteristics

Fig. 3 shows the typical NPF events observed at Pune (22 May 2012) and Kanpur (23 April 2013), and the hourly time evolution of particle size distributions, $D_{p,\ mode}$, temperature, RH, wind speed and direction, SO_2, solar radiation, N_{5-25}, and CS_{4-750}, on the respective event days. For these events, particle size distributions displayed a burst of ultrafine particles (visible above ~7 nm) and a sustained growth in size (Fig. 3a, c), and thus appearing as a conventional noontime "banana-shaped" size growth. These traditional "banana" events are typically observed when NPF occurs over a large spatial scale, indicative of regional NPF event (Kulmala et al., 2012). These typical events occurred at about 9:00 LT at both sites with increase in solar radiation, except that a small break at about 10:00 LT during the event at Kanpur site coinciding with a rapid change in wind direction (Fig. 3d). At about 9:00 LT, the N_{5-25} increased sharply from $(1–2) \times 10^3$ cm^{-3} to $(12–14) \times 10^3$ cm^{-3} at 12:00 LT, at both sites. A simultaneous increase in SO_2 was also observed at the Kanpur site, indicating the availability and uptake of H_2SO_4 (via SO_2 + OH reaction) for formation and subsequent growth of newly formed particles during an event. At about 6:00 LT, N_{5-25} increased sharply from ~1×10^3 cm^{-3} to ~6×10^3 cm^{-3} at Kanpur, with wind direction shifting from south-east to north-east. These are likely to be locally transported ultrafine particles from

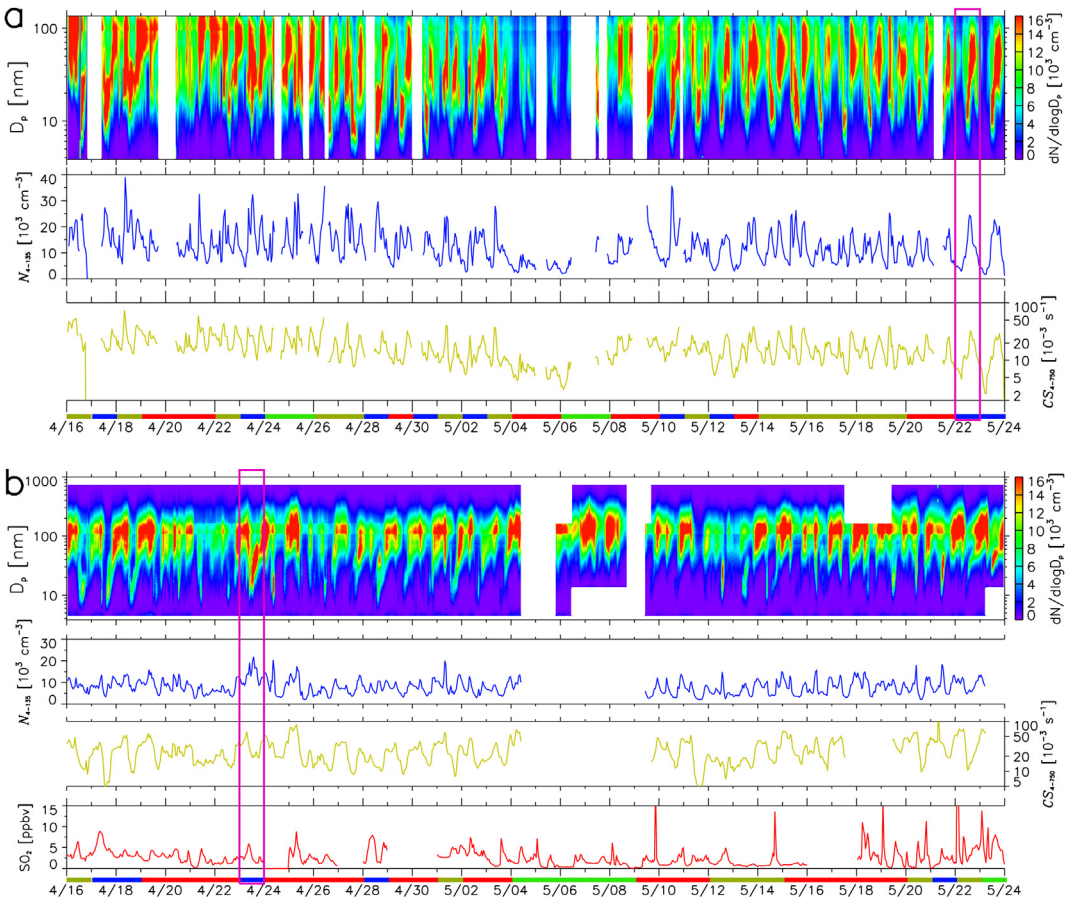

Fig. 2. Hourly time evolution of particle size distribution, N_{4-135}, CS_{4-750}, and SO_2 at (a) Pune during 16 April–23 May 2012 and (b) Kanpur during 16 April–23 May 2013. Note that there are no SO_2 and LDMA data available at the Pune site. The colored horizontal bars at the bottom indicate identified event types (blue = NPF, red = nonNPF, yellow = unidentified, and green = no data). The open rectangles indicate selected typical NPF events (Fig. 3) which are discussed in Section 3.1. (For interpretation of the references to color in this figure legend, the reader is referred to the web version of this article.)

vehicular emissions as a road with a moderately heavy traffic is located about 600 m to the East of the site.

On the contrary, the diurnal variation in condensation sink during NPF events was different between the sites. At Pune, CS_{4-750} showed less significant reduction before the start of NPF and then steadily increased during NPF, reaching a maximum in the late afternoon. At Kanpur, CS_{4-750} was significantly decreased before the start of NPF, possibly due to strong atmospheric dilution as a result of boundary layer evolution after sunrise, reaching a maximum at midnight. At about 9:00 LT, the CS_{4-750} was 33.6 $\times$ 10^{-3} s^{-1} and 10.4 $\times$ 10^{-3} s^{-1} at Kanpur and Pune, respectively. It appears that the NPF was not suppressed by the presence of large pre-existing particles at the Kanpur site, but it seemed to occur when the condensation sink was reduced sufficiently after sunrise. A sustained growth in size at Pune was completely ended at about 18:00 LT (~60 nm), whereas it continued until 22:00 LT at Kanpur, particles reaching ~80 nm. For these events, the mean GR and J_5 at Pune were 7.3 nm h^{-1} and 5.5 cm^{-3} s^{-1}, respectively. At Kanpur, these were 5.2 nm h^{-1}, and 3.2 cm^{-3} s^{-1}, respectively.

Fig. 4 shows the percentage frequency of NPF, nonNPF, unidentified event days and days on which no data was available at both sites during the campaigns. A total of 9 NPF events (26%) were observed out of 34 observation days at Pune, higher compared to that of 5 NPF events (14%) at Kanpur. A recent study at Pune also showed comparable NPF frequency in April–May (about 38% of available measurement days) (Siingh et al., 2013). Overall, the NPF

Table 1
The campaign mean, standard deviation (σ), median, minimum and maximum of particle number concentrations in different size ranges, CS_{4-750}, $D_{p,\,mode}$, and SO_2 at Pune and Kanpur based on hourly averaged data.

Parameter	Pune				Kanpur			
	Mean ± σ	Median	Min	Max	Mean ± σ	Median	Min	Max
N_{5-25} [10^3 cm^{-3}]	3.9 ± 3.5	2.9	0.015	24.2	0.9 ± 1.1	0.5	0.09	14.4
N_{25-100} [10^3 cm^{-3}]	8.2 ± 4.6	7.1	0.004	31.5	4.4 ± 2.2	3.9	0.8	16.9
$N_{100-750}$ [10^3 cm^{-3}]	–	–	–	–	2.8 ± 1.3	2.6	0.4	7.9
N_{4-135} [10^3 cm^{-3}]	12.2 ± 6.1	11.5	0.065	38.9	7.9 ± 3.4	7.5	0.2	23.1
CS_{4-750} [10^{-3} s^{-1}]	16.2 ± 7.1	–	–	–	33.3 ± 8.7	24.3	0.09	102.3
$D_{p,\,mode}$ [nm]	47.8 ± 22.1	46.1	5.3	>135	86.2 ± 39.1	82.6	9.2	162.5
SO_2 [ppbv]	–	–	–	–	2.53 ± 2.1	2.23	0.05	33.42

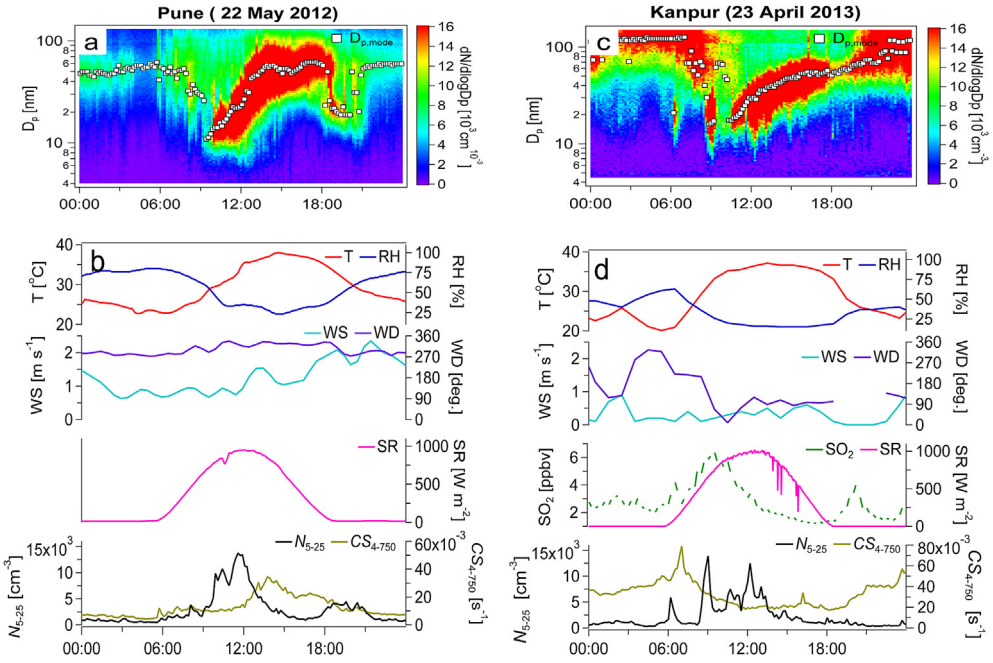

Fig. 3. Typical NPF event observed at Pune on 22 May 2012 (left panels) and at Kanpur on 23 April 2013 (right panels). The top panels show contour plot of particle size distributions superimposed with $D_{p,\,mode}$, and the bottom panels show time variation of temperature, RH, wind speed (WS), wind direction (WD), SO_2, solar radiation (SR), N_{5-25}, and CS_{4-750} during respective event days.

frequency at Pune and Kanpur was comparable to that in other urban areas in June–August months such as Beijing (Yue et al., 2009) and Pittsburgh (Stanier et al., 2004). The unidentified event days were further analyzed at both sites based on Buenrostro Mazon et al. (2009) classification. Based on particle size distributions characteristics alone, the observed 14 unidentified events at Pune can be broken into 8 nucleation-mode peak (57%), 4 tail (29%) and 2 unclassified (14%) event subtypes. At Kanpur, the observed 8 unidentified events can be broken into 4 nucleation-mode peak (50%) and 4 tail (50%) event subtypes (Fig. 4). Table 2 summarizes the derived *GR* and J_5 for all observed NPF events at both sites. The *GR* ranged from 3.4 to 7.6 nm h^{-1}, with a mean and standard deviation of 6.5 ± 1.2 nm h^{-1} at Pune, whereas it ranged from 5.2 to 13.3 nm h^{-1}, with a mean and standard deviation of 8.7 ± 3.2 nm h^{-1} at Kanpur. The derived *GR* at our sites was comparable to typical ranges observed in other urban areas; Brisbane (1.8–7.8 nm h^{-1}) (Cheung et al., 2011), Beijing (0.3–12.3 nm h^{-1}) (Yue et al., 2009), and Helsinki (1.9–9.4 nm h^{-1}) (Hussein et al., 2008), but slightly lower compared to that observed at Gaul Pahari in India (11.6–18.1 nm h^{-1}) (Mönkkönen et al., 2005). J_5 ranged from 3.5 to 13.9 cm^{-3} s^{-1}, with a mean and standard deviation of 7.2 ± 3.3 cm^{-3} s^{-1} at Pune, whereas it ranged from 0.4 to 3.2 cm^{-3} s^{-1}, with a mean and standard deviation of 1.5 ± 1.0 cm^{-3} s^{-1} at Kanpur. At Pune, these rates are comparable to typical ranges observed in other urban areas; Gual Pahari, India (J_3, 3.3–13.9 cm^{-3} s^{-1}) (Mönkkönen et al., 2005), Singapore (J_5, 5.8–43.5 cm^{-3} s^{-1}) (Betha et al., 2013) and Beijing (J_3, 4.5–19.3 cm^{-3} s^{-1}) (Yue et al., 2009), whereas these are lower at Kanpur compared to Pune as well as other urban areas. Several NPF studies reported the formation rate of ultrafine particles, but at different sizes, e.g. 1.5 nm ($J_{1.5}$) (Kulmala et al., 2013), 1.7 nm ($J_{1.7}$) (Kirkby et al., 2011), 3 nm (J_3) (Kulmala et al., 2004), or 5 nm (J_5) (Betha et al., 2013). This dissimilarity is attributed to the different measurable lower cut-off size of the instrument in these studies.

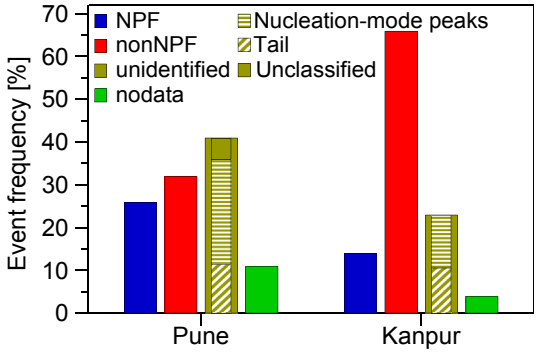

Fig. 4. Percentage frequency of NPF, nonNPF, unidentified event days and days on which no data was available at Pune and Kanpur sites. The subtypes of unidentified event days are also shown.

Table 2
Derived particle growth rate (*GR*), formation rate (J_5), and coagulation sink (F_{coag}) term for observed NPF events at both sites.

Date	*GR* [nm h^{-1}]	J_5 [cm^{-3} s^{-1}]	F_{coag} [cm^{-3} s^{-1}]
Pune			
17 April	6.5	9.7	8.5
23 April	6.1	13.9	11.9
28 April	6.9	3.9	3.5
30 April	3.4	4.7	4.4
02 May	7.6	6.6	5.2
10 May	5.8	11.0	9.5
12 May	7.2	3.5	2.5
22 May	7.3	5.5	4.2
23 May	6.4	6.1	5.6
Mean ± σ	6.5 ± 1.2	7.2 ± 3.3	6.2 ± 2.9
Kanpur			
April 17	8.7	0.8	0.5
April 18	11.1	0.4	0.2
April 23	5.2	3.2	2.7
April 28	6.9	1.8	1.2
May 21	13.3	1.4	0.6
Mean ± σ	8.7 ± 3.2	1.5 ± 1.0	1.0 ± 0.9

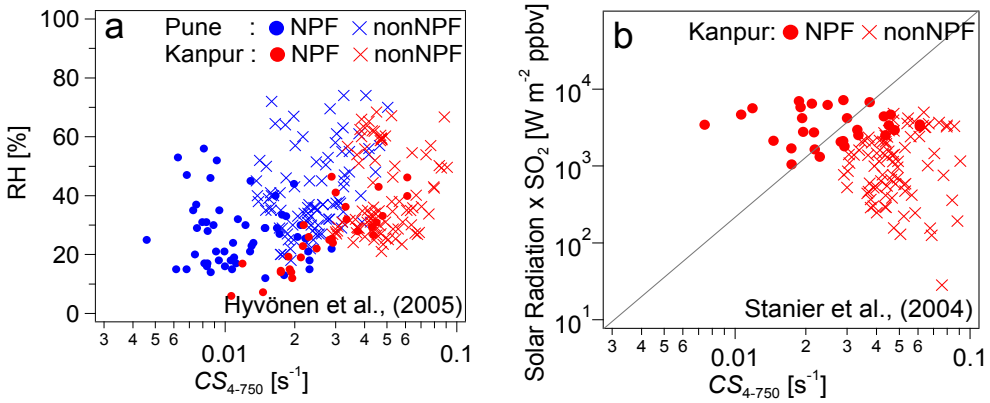

Fig. 5. Distribution of observed NPF and nonNPF events for nucleation occurrence methods, (a) Hyvönen et al. (2005) and (b) Stanier et al. (2004). Each data point indicates 10 min averaged value.

Since no existing nucleation theory is fully reliable to examine occurrence of NPF, a correlation between environmental variables may be a useful tool to understand whether the nucleation occurs or not under given atmospheric conditions. Here we used the methods described by Hyvönen et al. (2005) and Stanier et al. (2004). The former study suggested that the occurrence of NPF is linked to the relationship between RH and condensation sink, whereas the latter study suggested that the occurrence of NPF is linked to condensation sink (its increase prevents NPF), and a product of SO_2 and solar radiation (its increase favors NPF via H_2SO_4 production). For NPF event days, these parameters were chosen over a particular time period that a nucleation event is taking place. However, they were chosen from 8:00 to 16:00 LT on nonNPF event days. These parameters were then calculated at 10 min time interval for both event types. Fig. 5a shows scatter plot of CS_{4-750} versus RH during the NPF and nonNPF events at both sites. The condensation sink was found to grow with RH at both sites. But, there was no clear distinction between NPF and nonNPF event days for Hyvönen et al. (2005) method. In general, the relatively low *CS* and low RH values were the favorable conditions for NPF at both sites.

Further, the scatter plot of CS_{4-750} versus solar radiation $\times$ SO_2 during NPF and nonNPF events at Kanpur showed that the approach by Stanier et al. (2004) generally works for this site, as most NPF event days lie to the left of the diagonal line (Fig. 5b), indicating that low *CS* is needed together with high H_2SO_4 for NPF to occur. Note that the examination of these nucleation criteria for NPF event occurrence worked reasonably well in Kanpur, but they do not provide justifiable threshold value for NPF event occurrence, perhaps due to the omission of parameter (e.g. condensable organic vapor concentration) that has a significant contribution to nucleation and growth processes (Zhang et al., 2004). Further, the relative impact of each parameter might also vary with season (Boy and Kulmala, 2002). Fig. S3 shows the scatter plot of CS_{4-750} versus J_5 for all observed NPF events at Pune and Kanpur. A negative correlation of −0.6 was observed for both sites together, suggesting that particle nucleation is expected to be less favored in the urban areas due to a higher condensation sink. Contrarily, low condensation sink has been found to favor particle formation in rural areas, e.g. Hyytiälä, Finland (Kulmala et al., 2005). It seems that the characteristics of regional NPF events should be primarily linked to the origin and meteorological properties of the sampled air masses than the nature of the measurement site itself.

3.3. Effect of environmental parameters on NPF

The CS_{4-750} on NPF event days was smaller than that of nonNPF event days at both sites (Fig. 6a, f). Since, CS_{4-750} showed the same tendency at both sites; it appears to us that NPF was limited by large pre-existing particle surface area at these sites. Most studies showed that NPF is often associated with low *CS* (Dal Maso et al., 2005; Kanawade et al., 2012), because large background concentration of aerosols appears to consume condensable vapors and thus prevents NPF. However, NPF has also been observed in polluted environments under high *CS* conditions (Hamed et al., 2007; McMurry et al., 2005; Stanier et al., 2004), likely due to elevated source of condensable vapors to trigger NPF in these environments.

Aside from *CS*, NPF processes are also strongly influenced by various meteorological parameters. We have also calculated diurnal variation of RH, solar radiation, and temperature on NPF and nonNPF event days at both sites (Fig. 6b–d, g–i). The RH was generally lower on NPF event days than on nonNPF event days at both sites (Fig. 6b, g). Similar behavior was also reported by other studies in urban areas such as Melpitz (Birmili and Wiedensohler, 2000) and San Pietro Capofiume, Po Valley, Italy (Hamed et al., 2007). Thus, NPF appears to be suppressed at high RH perhaps due to enhanced coagulational scavenging of sub-3 nm clusters, weak gas-phase oxidation chemistry due to diminished solar radiation on cloudy days, and/or increased *CS* due to hygroscopic growth of the pre-existing particles (Hamed et al., 2011). Solar radiation is also an important parameter in the initial steps of nucleation, leading to formation of condensable species via active photochemical reactions. It was on average higher on NPF event days than on nonNPF event days (Fig. 6c, h). The temperature was generally higher on NPF event days than on nonNPF event days (Fig. 6d, i). While similar behavior was observed in east and south Germany (Birmili and Wiedensohler, 2000) in summer (June–August), the opposite behavior was also reported in clean areas such as Finland (Boy and Kulmala, 2002). Based on Mann–Whitney Wilcoxon *U*-Test, the differences between NPF and nonNPF events for *CS*, RH, solar radiation and temperature were statistically significant ($p \leq 0.05$) at Pune. These were significant for *CS*, RH and solar radiation, and insignificant for temperature ($p \geq 0.05$) at Kanpur. In general, nucleation events were observed at lower *CS*, lower RH, higher solar radiation, and higher temperature.

4. Conclusions

NPF characteristics were studied using particle size distribution measurements between 4 and 750 nm at two distinct urban locations in India. Particle number concentrations at Pune were higher than those observed at Kanpur, whereas the condensation sink was higher at Kanpur compared to that at Pune. This is because of higher anthropogenic sources of larger aerosol particles (e.g.

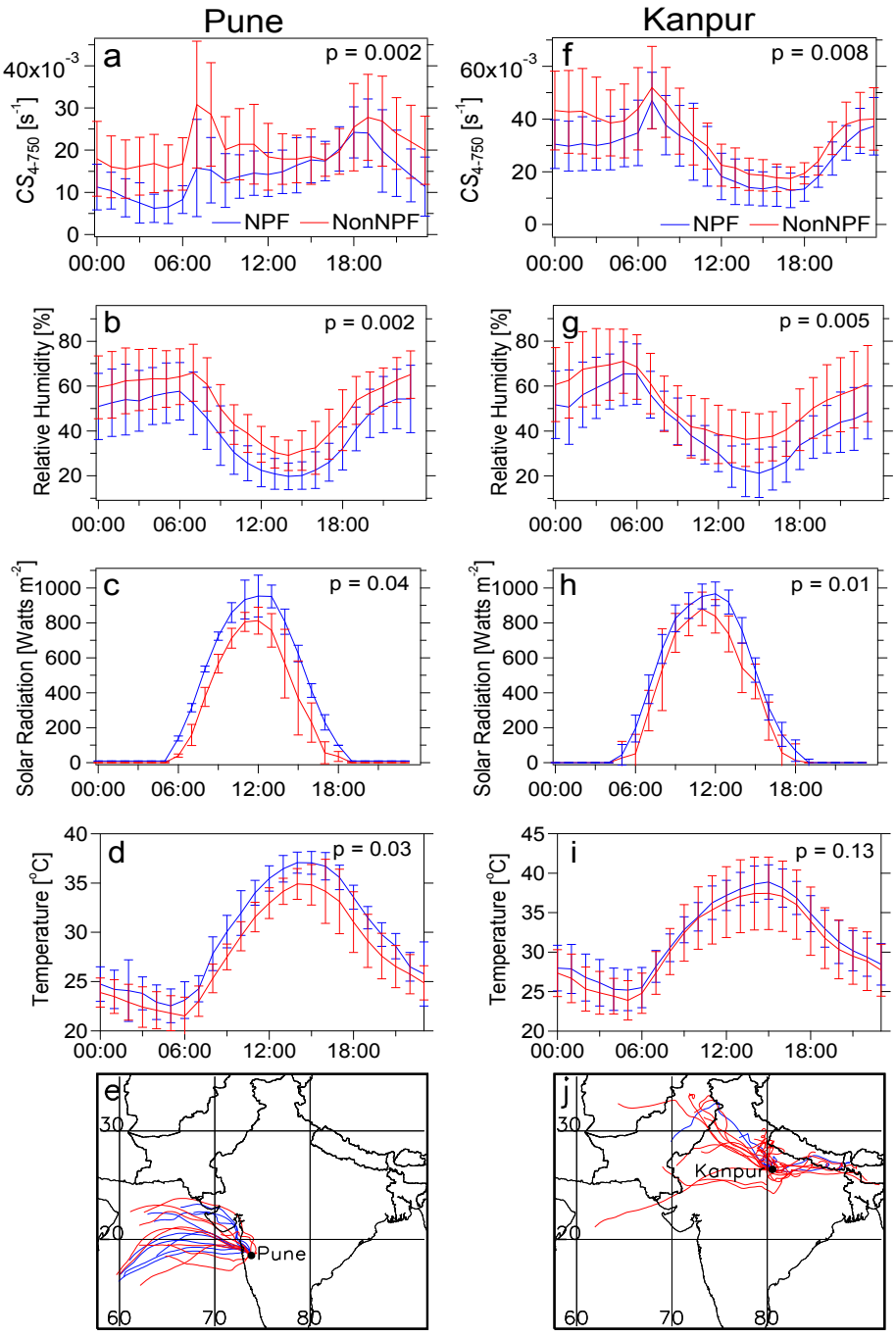

Fig. 6. Averaged diurnal variation in CS_{4-750}, RH, solar radiation, and temperature and air mass backward trajectories arriving at 100 m above the surface at 12:00 LT on NPF and nonNPF event days at Pune (a–e) and Kanpur (f–j). The error bars indicate standard deviation. The *p*-value indicates the two-tailed probability value at significance level of 0.05 for Mann–Whitney Wilcoxon *U*-Test.

biomass/biofuel burning and cooking, besides the traffic emissions) at Kanpur. The NPF frequency was higher at Pune (26%) than that at Kanpur (14%), both comparable to the observed frequency in summer (June–August) months globally (Kulmala et al., 2004; Yue et al., 2009; Stanier et al., 2004; Dal Maso et al., 2005). The derived *GR* and J_5 ranged from 3.4 to 13.3 nm h^{-1} and 0.4 to 13.9 cm^{-3} s^{-1}, respectively, which were also comparable to typical values reported in urban areas (Hussein et al., 2008; Mönkkönen et al., 2005; Yue et al., 2009). The particle formation rates were generally found higher at Pune, whereas the growth rates were higher at Kanpur. It seemed to us that the presence of pre-existing large particles at Kanpur than at Pune suppressed formation rates and favored particle growth. An examination of two nucleation criteria for NPF event occurrence indicated that lower *CS*, lower RH, and higher H_2SO_4 vapor source were the most favorable conditions for NPF to occur at these sites. A negative correlation ($R^2 = -0.6$) between the condensation sink and the particle formation rate for both sites together further suggested that particle nucleation can occur in urban environments when condensation sink is sufficiently reduced, consistent with previous study in India (Mönkkönen et al., 2005). Our results further indicated that NPF occurred at lower RH, higher solar radiation, and higher temperature. Nonetheless,

dedicated long-term NPF observations are crucial and required over Indian subcontinent, which has been largely unstudied so far.

Acknowledgments

SNT gratefully acknowledge the financial support given by the Earth System Science Organization, Ministry of Earth Sciences, Government of India (MOES/16/05/11-RDEAS) to conduct this research. This work in part is supported by National Academy of Sciences (NAS, 2000002802) and U. S. Agency for International Development (USAID, AID-OAA-A-11-00012). The views expressed here are of authors and do not necessarily reflect of NAS or USAID. Authors also thank B. N. Goswami (Director, IITM) for his support and encouragement during this study. AKK acknowledges the support under the INSA Senior Scientist Programme. We also acknowledge NOAA ARL for providing HYSPLIT air mass back trajectory calculations, ECCAD-Ether project of the GEIA database for providing REAS BC anthropogenic emissions, and University of Maryland for MODIS fire counts. We thank Gufran Beig and Huan Yu for fruitful discussions, and Anubhav Trivedi and Rosalin Dalai for technical assistance. We are also grateful to the anonymous referees's for constructive comments and suggestions which helped us to improve the overall quality of the manuscript.

Appendix A. Supplementary data

Supplementary data related to this article can be found at http://dx.doi.org/10.1016/j.atmosenv.2014.08.001.

References

Almeida, J., et al., 2013. Molecular understanding of sulphuric acid-amine particle nucleation in the atmosphere. Nature 502, 359–363.
Ball, S.M., Hanson, D.R., Eisele, F.L., McMurry, P.H., 1999. Laboratory studies of particle nucleation: initial results for H_2SO_4, H_2O, and NH_3 vapors. J. Geophys. Res. 104, 23709–23718.
Baron, P.A., Willeke, K., 2001. Aerosol Measurement: Principles, Techniques, and Applications, 2nd 466 ed. John Wiley and Sons, New York.
Betha, R., Spracklen, D.V., Balasubramanian, R., 2013. Observations of new aerosol particle formation in a tropical urban atmosphere. Atmos. Environ. 71, 340–351.
Birmili, W., Wiedensohler, A., 2000. New particle formation in the continental boundary layer: meteorological and gas phase parameter influence. Geophys. Res. Lett. 27, 3325–3328.
Boy, M., Kulmala, M., 2002. Nucleation events in the continental boundary layer: influence of physical and meteorological parameters. Atmos. Chem. Phys. 2, 1–16.
Buenrostro Mazon, S., et al., 2009. Classifying previously undefined days from eleven years of aerosol-particle-size distribution data from the SMEAR II station, Hyytiälä, Finland. Atmos. Chem. Phys. 9, 667–676.
Cheung, H.C., Morawska, L., Ristovski, Z.D., 2011. Observation of new particle formation in subtropical urban environment. Atmos. Chem. Phys. 11, 3823–3833.
Dal Maso, M., Kulmala, M., Riipinen, I., Wagner, R., Hussein, T., Aalto, P., Lehtinen, E.J., 2005. Formation and growth rates of fresh atmospheric aerosols: eight years of aerosol size distribution data from SMEARII, Hyytiälä, Finland. Boreal Environ. Res. 10, 323–336.
Dawson, M.L., Varner, M.E., Perraud, V., Ezell, M.J., Gerber, R.B., Finlayson-Pitts, B.J., 2012. Simplified mechanism for new particle formation from methanesulfonic acid, amines, and water via experiments and ab initio calculations. Proc. Natl. Acad. Sci. U. S. A. 109, 18719–18724.
Garg, A., Kapshe, M., Shukla, P.R., Ghosh, D., 2002. Large point source (LPS) emissions from India: regional and sectoral analysis. Atmos. Environ. 36, 213–224.
Hamed, A., Joutsensaari, J., Mikkonen, S., Sogacheva, L., Dal Maso, M., Kulmala, M., Cavalli, F., Fuzzi, S., Facchini, M.C., Decesari, S., Mircea, M., Lehtinen, K.E.J., Laaksonen, A., 2007. Nucleation and growth of new particles in Po Valley, Italy. Atmos. Chem. Phys. 7, 355–376.
Hamed, A., Korhonen, H., Sihto, S.-L., Joutsensaari, J., Jarvinen, H., Petaja, T., Arnold, F., Nieminen, T., Kulmala, M., Smith, J.N., Lehtinen, K.E.J., Laaksonen, A., 2011. The role of relative humidity in continental new particle formation. J. Geophys. Res. 116, D03202.
Hussein, T., Martikainen, J., Junninen, H., Sogacheva, L., Wagner, R., Dal Maso, M., Riipinen, I., Aalto, P.P., Kulmala, M., 2008. Observation of regional new particle formation in the urban atmosphere. Tellus B 60, 509–521.
Hyvärinen, A.P., Lihavainen, H., Komppula, M., Panwar, T.S., Sharma, V.P., Hooda, R.K., Viisanen, Y., 2010. Aerosol measurements at the Gual Pahari EUCAARI station: preliminary results from in-situ measurements. Atmos. Chem. Phys. 10, 7241–7252.
Hyvönen, S., et al., 2005. A look at aerosol formation using data mining techniques. Atmos. Chem. Phys. 5, 3345–3356.
Iida, K., Stolzenburg, M.R., McMurry, P.H., Smith, J.N., 2008. Estimating nanoparticle growth rates from size-dependent charged fractions: analysis of new particle formation events in Mexico City. J. Geophys. Res. 113, D05207.
Kanawade, V., Tripathi, S.N., 2006. Evidence for the role of ion-induced particle formation during an atmospheric nucleation event observed in Tropospheric Ozone Production about the Spring Equinox (TOPSE). J. Geophys. Res. 111, D02209.
Kanawade, V.P., Benson, D.R., Lee, S.-H., 2012. Statistical analysis of 4-year observations of aerosol sizes in a semi-rural Continental environment. Atmos. Environ. 59, 30–38.
Kanawade, V.P., et al., 2014. Infrequent occurrence of new particle formation at a semi-rural location, Gadanki, in tropical Southern India. Atmos. Environ. 94, 264–273.
Kaskaoutis, D.G., Singh, R.P., Gautam, R., Sharma, M., Kosmopoulos, P.G., Tripathi, S.N., 2012. Variability and trends of aerosol properties over Kanpur, northern India using AERONET data (2001–10). Environ. Res. Lett. 7, 024003.
Kirkby, J., et al., 2011. Role of sulphuric acid, ammonia and galactic cosmic rays in atmospheric aerosol nucleation. Nature 476, 429–433.
Komppula, M., Lihavainen, H., Hyvärinen, A.P., Kerminen, V.M., Panwar, T.S., Sharma, V.P., Viisanen, Y., 2009. Physical properties of aerosol particles at a Himalayan background site in India. J. Geophys. Res. 114, D12202.
Kulmala, M., dal Maso, M., Makela, J.M., Pirjola, L., Vakeva, M., Aalto, P., Miikkulainen, P., Hameri, K., O'Dowd, C.D., 2001. On the formation, growth, and composition of nucleation mode particles. Tellus 53B, 479–490.
Kulmala, M., et al., 2013. Direct observations of atmospheric aerosol nucleation. Science 339, 943–946.
Kulmala, M., Petäjä, T., Mönkkönen, P., Koponen, I.K., Dal Maso, M., Aalto, P.P., Lehtinen, K.E.J., Kerminen, V.-M., 2005. On the growth of nucleation mode particles: source rates of condensable vapor in polluted and clean environments. Atmos. Chem. Phys. 5, 409–416.
Kulmala, M., et al., 2012. Measurement of the nucleation of atmospheric aerosol particles. Nat. Protoc. 7, 1651–1667.
Kulmala, M., Vehkamäki, H., Petäjä, T., Dal Maso, M., Lauri, A., Kerminen, V.M., Birmili, W., McMurry, P.H., 2004. Formation and growth rates of ultrafine atmospheric particles: a review of observations. J. Aerosol Sci. 35, 143–176.
Lee, S.-H., Reeves, J.M., Wilson, J.C., Hunton, D.E., Viggiano, A.A., Miller, T.M., Ballenthin, J.O., Lait, L.R., 2003. Particle formation by ion nucleation in the upper troposphere and lower stratosphere. Science 301, 1886–1889.
McMurry, P.H., et al., 2005. A criterion for new particle formation in the sulfur-rich Atlanta atmosphere. J. Geophys. Res. 110, D22S02.
Mejía, J.F., Morawska, L., 2009. An investigation of nucleation events in a coastal urban environment in the Southern Hemisphere. Atmos. Chem. Phys. 9, 7877–7888.
Merikanto, J., Spracklen, D.V., Mann, G.W., Pickering, S.J., Carslaw, K.S., 2009. Impact of nucleation on global CCN. Atmos. Chem. Phys. 9, 8601–8616.
Metzger, A., et al., 2010. Evidence for the role of organics in aerosol particle formation under atmospheric conditions. Proc. Natl. Acad. Sci. U. S. A. 107, 6646–6651.
Mönkkönen, P., Koponen, I.K., Lehtinen, K.E.J., Hämeri, K., Uma, R., Kulmala, M., 2005. Measurements in a highly polluted Asian mega city: observations of aerosol number size distribution, modal parameters and nucleation events. Atmos. Chem. Phys. 5, 57–66.
Moorthy, K.K., et al., 2011. Fine and ultrafine particles at a near–free tropospheric environment over the high-altitude station Hanle in the Trans-Himalaya: new particle formation and size distribution. J. Geophys. Res. 116, D20212.
Neitola, K., Asmi, E., Komppula, M., Hyvärinen, A.-P., Raatikainen, T., Panwar, T.S., Sharma, V.P., Lihavainen, H., 2011. New particle formation infrequently observed in Himalayan foothills – why? Atmos. Chem. Phys., 8447–8458.
O'Dowd, C.D., AAlto, P., Hameri, K., Kulmala, M., Hoffmann, M.R., 2002. Atmospheric particles from organic vapors. Nature 416, 497–498.
Paasonen, P., et al., 2012. On the formation of sulphuric acid – amine clusters in varying atmospheric conditions and its influence on atmospheric new particle formation. Atmos. Chem. Phys. 12, 9113–9133.
Pierce, J.R., Adams, P.J., 2009. Uncertainty in global CCN concentrations from uncertain aerosol nucleation and primary emission rates. Atmos. Chem. Phys. 9, 1339–1356.
Schobesberger, S., et al., 2013. Molecular understanding of atmospheric particle formation from sulfuric acid and large oxidized organic molecules. Proc. Natl. Acad. Sci. U. S. A. 110, 17223–17228.
Schwartz, S.E., 1996. The whitehouse effect – shortwave radiative forcing of climate by anthropogenic aerosol: an overview. J. Aerosol Sci. 27, 359–382.
Seinfeld, J.H., Pandis, S.N., 2006. Atmospheric Chemistry and Physics: From Air Pollution to Climate Change, second ed. John Wiley and Sons. Inc, New York.
Sharma, N., Kuniyal, J., Singh, M., Sharma, P., Chand, K., Negi, A., Sharma, M., Thakur, H., 2011. Atmospheric ultrafine aerosol number concentration and its correlation with vehicular flow at two sites in the western Himalayan region: Kullu-Manali, India. J. Earth Syst. Sci. 120, 281–290.
Siingh, D., Gautam, A.S., Kamra, A.K., Komsaare, K., 2013. Nucleation events for the formation of charged aerosol particles at a tropical station – preliminary results. Atmos. Res. 132–133, 239–252.

Sipilä, M., Berndt, T., Petäjä, T., Brus, D., Vanhanen, J., Stratmann, F., Patokoski, J., Mauldin, R.L., Hyvärinen, A.-P., Lihavainen, H., Kulmala, M., 2010. The role of sulfuric acid in atmospheric nucleation. Science 327, 1243–1246.
Sogacheva, L., Hamed, A., Facchini, M.C., Kulmala, M., Laaksonen, A., 2007. Relation of air mass history to nucleation events in Po Valley, Italy, using back trajectories analysis. Atmos. Chem. Phys. 7, 839–853.
Spracklen, D.V., et al., 2008. Contribution of particle formation to global cloud condensation nuclei concentrations. Geophys. Res. Lett. 35, L06808.
Srivastava, A.K., Tripathi, S.N., Dey, S., Kanawade, V.P., Tiwari, S., 2012. Inferring aerosol types over the Indo-Gangetic Basin from ground based sunphotometer measurements. Atmos. Res. 109–110, 64–75.
Stanier, C.O., Kylstov, A.Y., Pandis, S.N., 2004. Nucleation events during the Pittsburgh air quality study: description and relation to key meteorological, gas phase, and aerosol parameters. Aerosol Sci. Tech. 38, 253–264.
Twomey, S., 1991. Aerosols, clouds, and radiation. Atmos. Environ. 25, 2435–2442.
Vakkari, V., Laakso, H., Kulmala, M., Laaksonen, A., Mabaso, D., Molefe, M., Kgabi, N., Laakso, L., 2011. New particle formation events in semi-clean South African savannah. Atmos. Chem. Phys. 11, 3333–3346.
Yu, F., Turco, R.P., 2008. Case studies of particle formation events observed in boreal forests: implications for nucleation mechanisms. Atmos. Chem. Phys. 8, 6085–6102.
Yu, H., McGraw, R., Lee, S.-H., 2011. Effects of amines on formation of sub-3 nm particles and their subsequent growth. Geophys. Res. Lett. 39, L02807.
Yue, D., Hu, M., Wu, Z., Wang, Z., Guo, S., Wehner, B., Nowak, A., Achtert, P., Wiedensohler, A., Jung, J., Kim, Y.J., Liu, S., 2009. Characteristics of aerosol size distributions and new particle formation in the summer in Beijing. J. Geophys. Res. 114, D00G12.
Zhang, R., 2010. Getting to the critical nucleus of aerosol formation. Science 328, 1366–1367.
Zhang, R., Suh, J., Zhao, J., Zhang, D., Fortner, E.C., Tie, X., Molina, M.T., Molina, M.J., 2004. Atmospheric new particle formation enhanced by organic acids. Science 304, 1487–1490.